nature communications

Article

https://doi.org/10.1038/s41467-024-54473-x

Redox-switchable multicolor luminescent polymers for theragnosis of osteoarthritis

Received: 6 January 2024

Accepted: 13 November 2024

Published online: 21 November 2024

Check for updates

Chuan Peng[1,3], Yuling Zhu[1,3], Kaibo Zhang[2], Yiwei Wang[1], Yi Zheng[1], Yang Liu[1], Weili Fu[2] ✉, Hong Tan[1], Qiang Fu[1] & Mingming Ding[1] ✉

Nonaromatic and nonconjugated fluorescent materials have garnered increasing attention in recent years. However, most non-classical chromophores are derived from electro-rich nitrogen and oxygen atoms, which suffer from short emission wavelengths, low efficiency, limited responsiveness, and obscure luminescence mechanisms. Here we present an emission mechanism in bioactive polycysteine, an aliphatic polymer that displays polymerization- and aggregation-induced emission, high quantum yield, and multicolor emission properties. We show that the hydrogen atoms bonded to the sulfur atoms play a crucial role in luminescence. This enables reversible modulation of polymer fluorescence under reducing and oxidizing conditions, facilitating specific imaging and quantitative detection of redox species in cells and in vivo. Furthermore, the polymer exhibits better anti-inflammatory and anti-oxidative activities compared to first-line clinical antioxidants, offering a promising platform for in vivo theragnosis of diseases such as osteoarthritis.

Many biological macromolecules display fluorescent properties in nature. One of the most prominent example is green fluorescent protein (GFP), which was first isolated from jellyfish and has since become a ubiquitous biomarker and imaging tool for studying protein localization and gene expression[1,2], revealing the molecular mechanisms of various biological processes[3]. Another example is cytochrome c, a mitochondrial protein that emits fluorescence when it forms aggregates under certain conditions[4], serving as a valuable probe for apoptosis and autophagy research[5,6]. Inspired by these fluorophores, synthetic luminescent polymers have been developed for various applications, such as imaging[7], biosensing[8], optoelectronics[9], metal ion and small molecule detection[10], and anti-counterfeiting[11]. Nonetheless, most of these polymers are depend on π-aromatic building units as the emitting centers, which pose challenges such as complicated synthesis, poor water solubility, and potential toxicity.

Alternatively, nonaromatic and nonconjugated fluorescent materials without conventional chromophores have attracted increasing attention in recent years. These materials have advantages such as molecular flexibility, superior processability, excellent biocompatibility, and biodegradability[12]. They usually rely on electron-rich heteroatoms with lone-pair electrons or isolated unsaturated bonds as the luminescent units[13]. However, the fundamental mechanism of their nonconventional luminescence remains largely elusive[14]. Moreover, these materials often exhibit low fluorescence quantum yields (QY) and emit in the ultraviolet range, and lack responsiveness and bioactivity, which limit their in vivo applications. To our knowledge, there are no reports on the use of nonclassical aliphatic fluorescent polymers for disease diagnosis and treatment in vivo.

In this work, we report a polycysteine (PCys) derived from natural amino acids that exhibited intrinsic fluorescence and color switching properties (Fig. 1a). The copolymer displays thiol-chromogenic and molecular weight dependent fluorescence with a high QY of up to 51.6%, as well as typical aggregation-induced emission (AIE) characteristics and multicolor luminescence. Moreover, the polythiol structure offers abundant active sites for redox reactions and potential antioxidative function. Notably, the fluorescence can be reversibly switched off by thiol oxidation and on by reduction, allowing the polymer to act as a multifunctional on-off sensor for intracellular or in vivo quantification of reactive oxygen species (ROS) and glutathione (GSH). Additionally, the bioactive polymer can be used as a drug-free

[1]College of Polymer Science and Engineering, State Key Laboratory of Polymer Materials Engineering, Sichuan University, Chengdu, China. [2]Sports Medicine Center, Department of Orthopedic Surgery and Orthopedic Research Institute, West China Hospital, Sichuan University, Chengdu, Sichuan, China. [3]These authors contributed equally: Chuan Peng, Yuling Zhu. ✉e-mail: foxwin2008@163.com; dmmshx@scu.edu.cn

https://doi.org/10.1038/s41467-024-54473-x

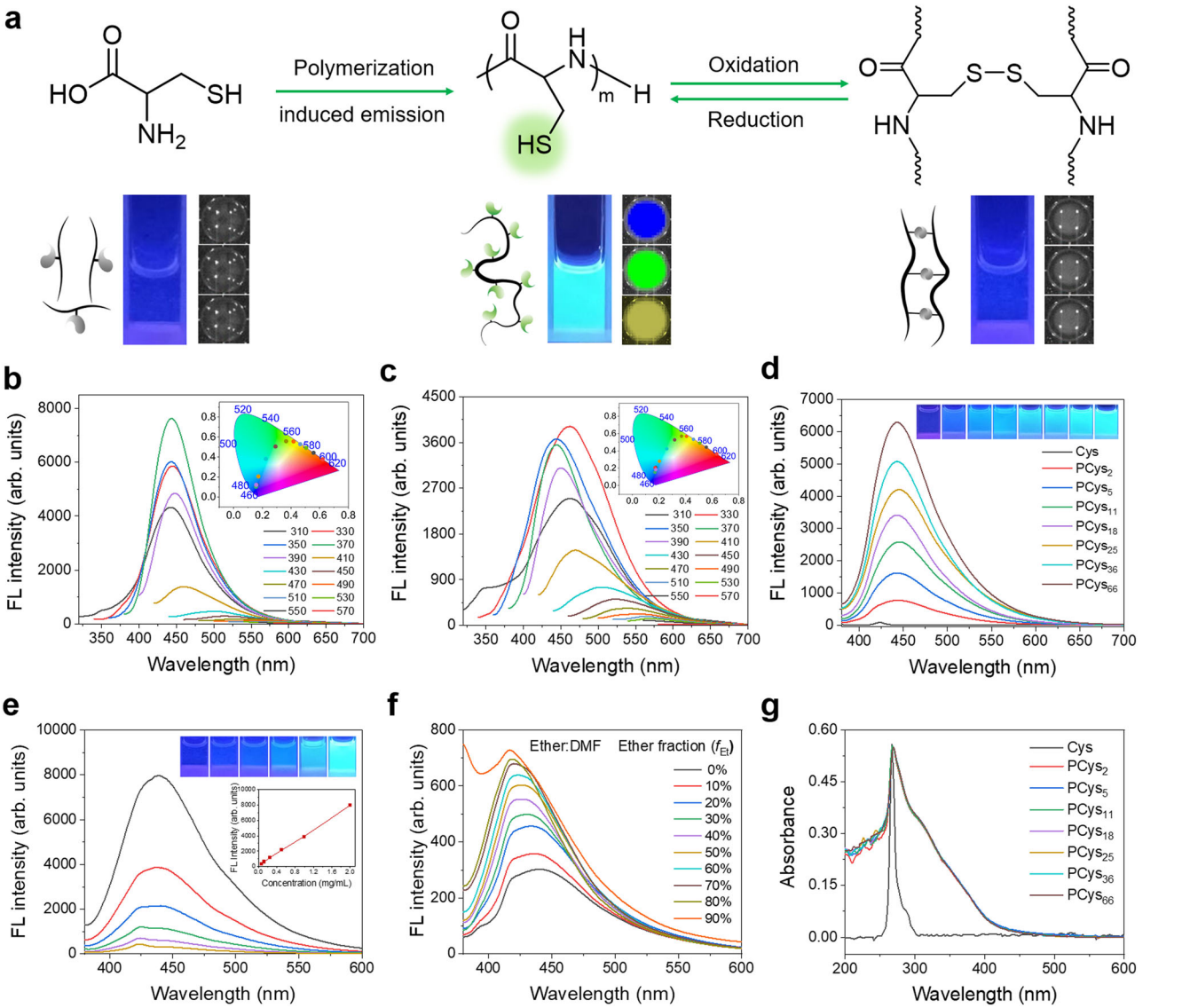

Fig. 1 | Design strategies and photophysical properties of fluorescent PCys. **a** The chemical structure of Cys, PCys and PCys-s as well as their fluorescence images under different excitation wavelengths (up to down: λ_{ex} = 415, 465, and 570 nm). **b**, **c** Fluorescence spectra of PCys in H_2O (**b**) and DMF (**c**) at different excitation wavelengths. CIE coordinates of PCys obtained at different excitation. **d** Photographs taken under 365 nm UV light and fluorescence spectra of $PCys_2$, $PCys_5$, $PCys_{11}$, $PCys_{18}$, $PCys_{25}$ $PCys_{36}$ and $PCys_{66}$ at the same thiol content. **e** Photographs taken under 365 nm UV light and fluorescence spectra of PCys in H_2O (λ_{ex} = 370 nm) with different concentrations. **f** Fluorescence spectra of PCys in ether/DMF mixed solvents with different ether fractions (f_{Et}) (λ_{ex} = 370 nm). **g** UV-vis spectra of Cys, $PCys_2$, $PCys_5$, $PCys_{11}$, $PCys_{18}$, $PCys_{25}$, $PCys_{36}$ and $PCys_{66}$ at the same thiol content.

and self-reporting system for diagnosis and antioxidant therapy of osteoarthritis in vivo.

Results

Synthesis of PCys

We first synthesized a carbobenzoxy modified L-cysteine-N-carboxylic anhydride (L-Cys-Cbz NCA) from L-Cys-Cbz using the Fuchs-Farthing method (Supplementary Figs. 1 and 2) and then performed ring-opening polymerizations (ROPs) of L-Cys-Cbz NCA with methoxypolyethylene glycol amine (MPEG-NH_2, MW 5000) in anhydrous *N,N*-Dimethylformamide (DMF) to produce MPEG-PCys-Cbz with controlled molecular weights and narrow molecular-weight distributions (Supplementary Fig. 3 and Table 1). The degrees of polymerization (DPs) ranged from 2 to 66 as calculated from the integration of the proton nuclear magnetic resonance spectra (^{1}H NMR, Supplementary Fig. 4 and Table 1). Next, we deprotected the Cbz group to obtain MPEG-PCys with thiol moieties. For clarity, the polymers were named $PCys_x$, where x is the number of cysteine residues per chain. The successful synthesis of $PCys_x$ was confirmed by ^{1}H NMR and Fourier transform infrared spectroscopy (FTIR, Supplementary Figs. 5 and 6). The thiol group contents of the polymers were quantified with an Ellman's reagent (5,5′-dithiobis-(2-nitrobenzoic acid), DTNB)[15] (Supplementary Fig. 7). Based on a cysteine standard curve (Supplementary Fig. 8), the numbers of thiol groups per chain were calculated to be 2.3, 4.7, 11.2, 18.3, 24.8, 36.4 and 65.8 for $PCys_2$, $PCys_5$, $PCys_{11}$, $PCys_{18}$, $PCys_{25}$, $PCys_{36}$ and $PCys_{66}$, respectively, which agree well with the ^{1}H NMR result.

Thiol luminophores: fluorescent properties and mechanism

Previous studies have demonstrated that electron-rich nitrogen or oxygen moieties can potentially form cluster chromophores and emit intrinsic fluorescence[16]. Sulfur, another electron-rich element with a larger atomic radius, has yet to be explored for its luminescent potential[17]. In addition, the role of the hydrogen atoms attached to

https://doi.org/10.1038/s41467-024-54473-x

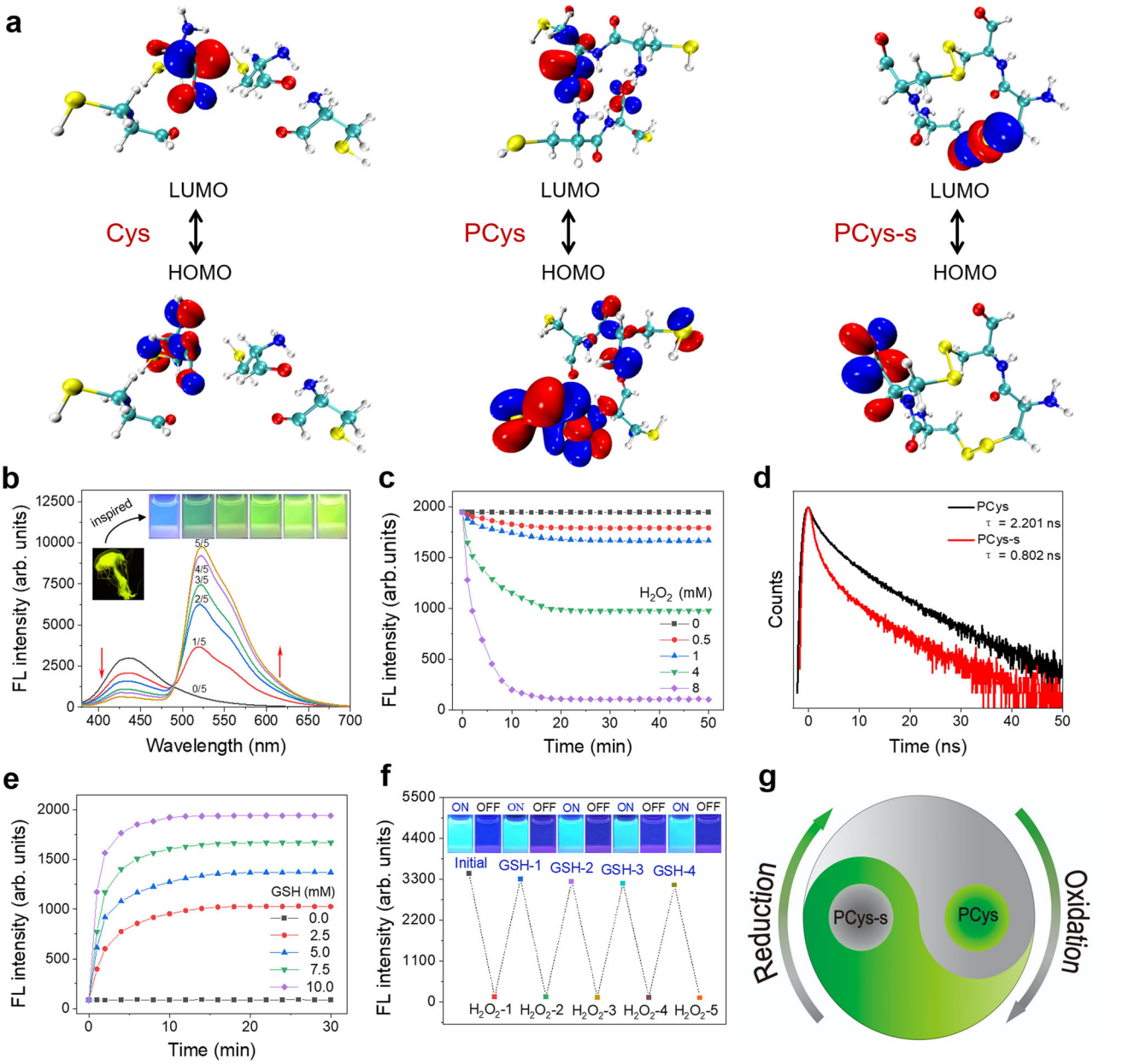

Fig. 2 | Mechanism and redox properties of fluorescence. a Electron distributions and energy states of Cys, PCys and PCys-s, respectively, calculated using TD-DFT at the level of B3LYP/6-31 G(d). **b** Fluorescence spectra of FITC-labeled PCys assemblies with different dye contents (FITC/PCys). Insets show a photograph of jellyfish, and the fluorescent images of assemblies under 365 nm UV light illumination. **c** Concentration-dependent changes in emission intensity during the incubation of PCys in H_2O with H_2O_2 (0-8 mM) for 50 min (λ_{ex} = 370 nm). **d** Fluorescence lifetimes for PCys and PCys-s (λ_{ex} = 370 nm). **e** Concentration-dependent changes in emission intensity during the incubation of PCys-s in H_2O with GSH (0-10 mM) for 30 min (λ_{ex} = 370 nm). **f** Photographs captured under 365 nm UV light and the reversible cycle response of PCys fluorescence when exposed to H_2O_2 and GSH (λ_{ex} = 370 nm). **g** Schematic illustration of the redox-switchable fluorescence of PCys.

these electronegative elements in non-classical luminescence has not been addressed. Here we show that PCys exhibits strong visible fluorescence (λ_m ~ 462 nm) under UV irradiation in various forms, including solid, solution, and water dispersion (Supplementary Figs. 9 and 10). This phenomenon is unexpected since non-traditional chromogenic polymers such as poly(amino acid)s and polypeptides generally do not emit fluorescence in aqueous environments[18]. More intriguingly, PCys in water exhibited a significant enhancement of fluorescence intensity and a red shift of optimal excitation wavelength compared with that in DMF (Supplementary Fig. 11), which may be attributed to the self-assembly of copolymer in water that facilitated the aggregation of PCys segments. Dynamic laser scattering (DLS) and transmission electron microscopy (TEM) measurements reveal that $PCys_x$ self-assembled into spherical nanoparticles with diameters ranging from 25 to 160 nm with a unimodal distribution (Supplementary Figs. 12, 13 and Supplementary Table 2). The variation in particle diameter is influenced by factors such as the hydrophilic/hydrophobic ratio, polymer conformation, intermolecular interactions and the aggregation number of the polymers[19–23]. Owing to the intrinsic fluorescence, the well-distributed spherical polymeric assemblies were also visualized in a label-free manner using confocal laser scanning microscopy (CLSM). Notably, the nanoparticles displayed diverse fluorescent colors under different excitation wavelengths (Supplementary Fig. 14), indicating that PCys can emit multicolor

fluorescence. The multicolor emission was also verified by the excitation-dependent fluorescence spectra of PCys in both DMF and H_2O (Fig. 1b, c and Supplementary Figs. 15 and 16). The emission peaks shifted to longer wavelengths as the excitation wavelength increased and reached up to 600 nm, which is beneficial for biomedical applications.

We hypothesize that the non-classical fluorescence of PCys originated from the polymerization of thiol groups, as cysteine itself is non-luminescent and PCys showed strong emission (Fig. 1d, Supplementary Fig. 17). To test this hypothesis, we first examined the fluorescence properties of PCys with different molecular weights at fixed thiol content. We found that the emission intensity and QY of PCys increased with the chain length (Fig. 1d), indicating a polymerization-induced emission (PIE) effect. At the degree of polymerization of 66, PCys exhibited a QY of 51.6% (Supplementary Fig. 18), which was more than ten times higher than those of chromophores containing only sulfur atoms (4.5%)[24]. This QY could be further enhanced by increasing the molecular weights. Notably, there is a strong linear correlation between fluorescence intensity and both the degree of polymerization and polymer concentration in water (Fig. 1e and Supplementary Fig. 19), irrespective of variations in particle diameter (Supplementary Figs. 12, 13 and Supplementary Table 2). These findings indicate that the fluorescence intensity of PCys is primarily influenced by the degree of polymerization and the content of thiol groups, with minimal impact from the particle size of the self-assembled structures. Furthermore, the addition of diethyl ether to a solution of PCys in DMF resulted in a more than threefold increase in fluorescence intensity as the diethyl ether fraction rose from 0 to 90% (Fig. 1f). This observation is indicative of typical AIE behavior. The polymerization of cysteine is an entropy-reduction process characterized by chain entanglement and intra- and interchain interactions, which are further strengthened by molecular aggregation, thereby bringing the thiol groups into closer proximity and facilitating through-space conjugation (TSC) interactions. The TSC interactions lead to the formation of clusters with extended electron delocalization and result in clusterization-triggered emission of PCys[25]. The non-classical clustered chromophore was also confirmed by ultraviolet-visible (UV-vis) spectra (Fig. 1g), where PCys showed a broad absorption peak from 300 to 450 nm compared to the Cys monomer, indicating that thiol polymerization produced the chromophore and induced luminescence.

To elucidate the fluorescence mechanism of PCys, we performed time-dependent density functional theory (TD-DFT) simulations at the B3LYP/6-31 G(d) level of theory[26]. We compared two systems: one with four cysteine molecules (Cys) and another with two dimers (PCys). The results revealed that electronic transitions occurred near the thiol groups of PCys, suggesting that the luminescence originated from the thiols (Fig. 2a). Next, we simulated the excited-state frontier molecular orbitals of Cys and PCys, including the highest occupied molecular orbitals (HOMO) and lowest unoccupied molecular orbitals (LUMO). The results showed that the HOMO-LUMO gap decreased upon polymerization, where the energy gaps of Cys and PCys were 3.758 and 2.325 eV, respectively (Supplementary Table 3), indicating that PCys had a lower excitation energy. Therefore, we reasoned that the polymerization reduced the distance between the discrete sulfhydryl groups, enhanced the electron delocalization and electron cloud overlap, increased TSC interactions, and thus lowered the energy gap and facilitated the electron transition and luminescence generation[27,28].

On the other hand, one may ask whether the backbone hydrogen bonding (H-bonding) interactions of peptide chains contributed to the photoluminescence performance of PCys, as H-bond-promoted emission has been reported for ionic fluorophores and peptidomimetic polymers[29,30]. To answer the question, we treated the PCys assemblies with lithium chloride (LiCl) and urea (Supplementary Fig. 20), which are known to disrupt H-bonds[31,32]. We found that the addition of these H-bond breakers did not affect the fluorescent spectra of PCys, thus ruling out the role of backbone H-bonds in the luminescence mechanism. Moreover, we examined whether the protonation state of thiol groups influenced their fluorescent properties. We recorded the fluorescence spectra of PCys at different pH values. It was found that the fluorescence intensity first increased and then decreased moderately with increasing pH value (Supplementary Fig. 21). The strongest emission was observed at ~pH 8.2, which was very close to the pKa of thiol groups (8.4)[33]. The result suggests that both protonation and ionization may adversely affect the luminescence capacity of thiol aggregates. In addition, it is known that thiol groups exhibit high reactivity and instability under oxidative conditions, potentially limiting the storage and application of PCys. To address this concern, we monitored the fluorescence changes of PCys in both aqueous solution and DMF over time. Encouragingly, the polymers did not show noticeable fluorescence variation after 48 h of exposure to air in H_2O (Supplementary Fig. 22a). In contrast, the fluorescence of PCys in DMF was significantly reduced (Supplementary Fig. 22b). Concurrently, DTNB analysis revealed no significant decrease in thiol content during incubation in H_2O, whereas the thiol content in DMF decreased markedly (Supplementary Fig. 23). Two factors likely contribute to the enhanced stability of PCys in aqueous solution. First, the self-assembly process encapsulated thiol moieties within a hydrophobic microenvironment, which resembled life systems that stabilize and regulate active sites through hydrophobic encapsulation induced by protein folding[34,35]. Second, the relatively low solubility and diffusion rate of oxygen in water reduced the likelihood of its interaction with the thiol groups[36,37]. Interestingly, PCys can also transfer its energy to conjugated fluorescein isothiocyanate isomer I (FITC) probe upon irradiation and result in yellow emissions (Fig. 2b). The fluorescence resonance energy transfer (FRET) behavior is quite similar to that of yellow fluorescence proteins (YFP)[38]. This study presents an example of polymers based on thiol fluorophores, offering a distinct class of luminescent materials and providing valuable insight into non-classical fluorescence phenomena.

Redox-switchable polymer sensor

Proteins in organisms are rich in thiols and can modulate their physiological activity through thiol-disulfide exchange reactions[39–41]. Inspired by this, we hypothesized that the oxidation of thiol groups to disulfide linkages may affect the luminescence behavior of PCys. To test this hypothesis, the polymeric assemblies were treated with different concentrations of hydrogen peroxide (H_2O_2). As expected, the fluorescence intensity of the solutions rapidly quenched upon oxidation and reached equilibrium within 15 min (Fig. 2c). The quenching rate was linearly correlated with H_2O_2 concentrations, and the emission almost vanished in the presence of 8 mM of H_2O_2. The fluorescence quench was also confirmed by a significant decrease of lifetime from 2.201 to 0.802 ns (Fig. 2d). FTIR spectra verified the disappearance of thiol groups and emergence of disulfide-linked copolymers (PCys-s) upon oxidation (Supplementary Fig. 24). Furthermore, we observed a notable reduction in the UV-vis absorption band between 300-450 nm following oxidation (Supplementary Fig. 25), indicative of chromophore disruption. These fundings reinforce the concept that thiol groups are the origin of luminescence, while disulfide is nonfluorescent. To elucidate the fluorescence quenching mechanism, we conducted TD-DFT calculations on the excited-state frontier molecular orbitals of PCys-s (Fig. 2a and Supplementary Table 3). The result revealed a larger energy in PCys-s compared to PCys, suggesting a decreased excitability. Moreover, we noticed a substantial modification in the electron cloud density surrounding the sulfur atom in oxidized PCys, implying that the hydrogen atom played a vital role in the emission process. Further investigation is required to elucidate the specific mechanisms of hydrogen atoms and their roles in other chromophores.

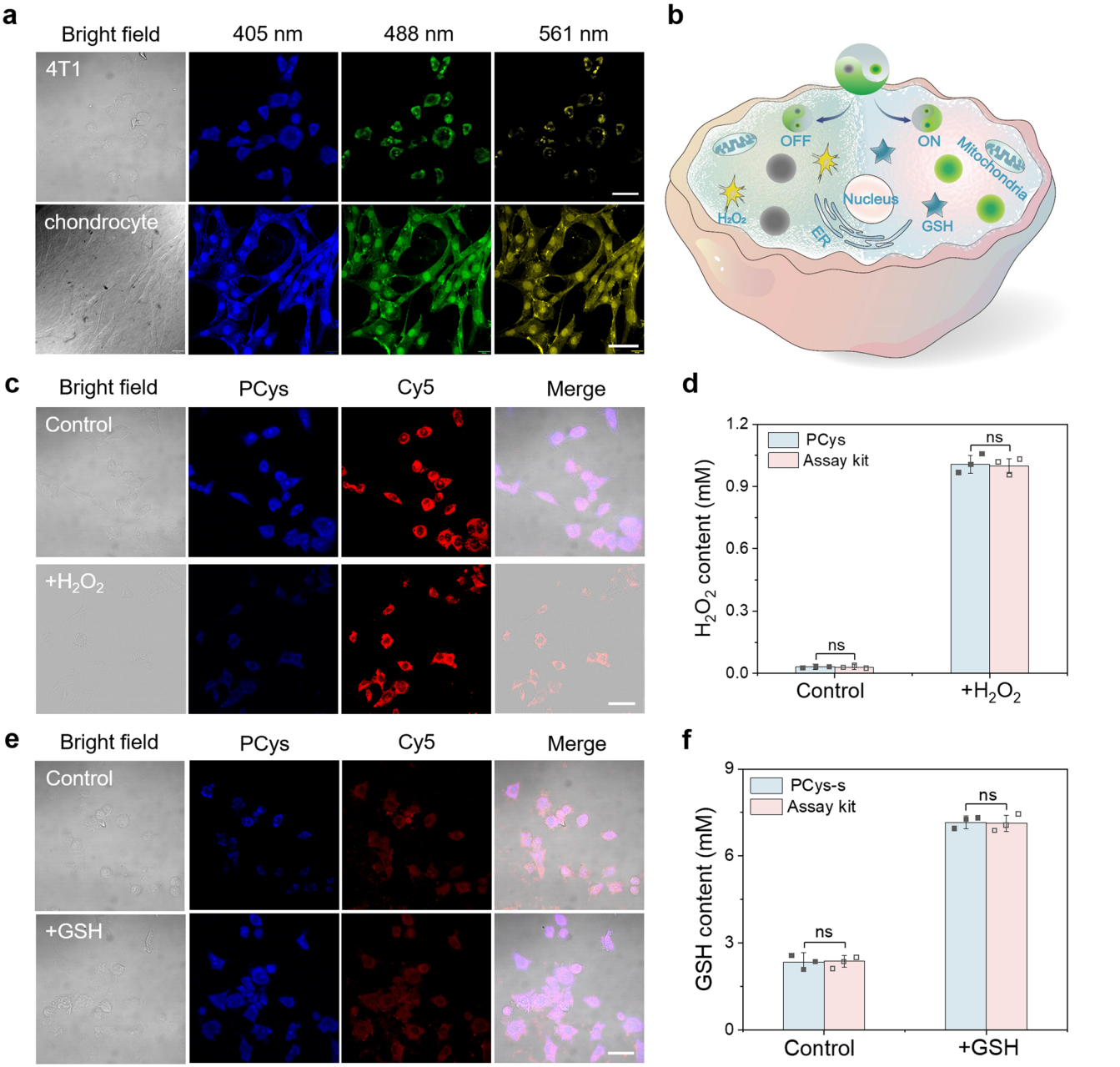

Fig. 3 | Multicolor cell imaging and quantitative detection of redox substances. **a** CLSM images of 4T1 cells and chondrocytes after 2 h of incubation with PCys (λ_{ex} = 405, 488, and 561 nm). **b** Schematic illustration of PCys detecting H_2O_2 and GSH in cells (ER: endoplasmic reticulum). **c** CLSM images of H_2O_2-pretreated or untreated 4T1 cells incubated with PCys-Cy5 for 2 h. **d** H_2O_2 levels in 4T1 cells with or without H_2O_2 pretreatment detected by PCys or H_2O_2 assay kit. **e** CLSM images of GSH-pretreated or untreated 4T1 cells incubated with PCys-s-Cy5 for 2 h. **f** GSH levels in 4T1 cells with or without GSH pretreatment detected by PCys-s or GSH assay kit. The scale bars in a, c, and e are 50 μm. Data are presented as the mean with SD (n = 3 independent cells) in (**d**, **f**). Statistical differences were analyzed by a one-way ANOVA with Tukey's multiple comparisons test. ns means no significance. Each experiment was repeated three times independently with similar results.

Considering the reversibility of thiol-disulfide exchange reaction, we further reasoned that the reductive cleavage of disulfide linkage would recover the fluorescence of copolymers. To validate this hypothesis, we added glutathione (GSH) to the oxidized polymer solution. We observed that the polymer fully restored its fluorescence within 10 min (Fig. 2e). More interestingly, the quenching and recovery of fluorescence were reversible and could be repeated multiple times by alternately adding H_2O_2 and GSH (Fig. 2f and Supplementary Movie 1). The redox reactions were further accelerated in non-assembled polymer solutions (Supplementary Fig. 26). These results demonstrate that PCys can serve as an "on-off" switchable fluorescent probe for quantitative detection of redox substances (Fig. 2g). To exploit this potential, we constructed ratiometric fluorescence probes by labeling the polymers with a redox-insensitive 3,3′-diethylthiadicarbocyanine iodide (Cy5) dye. The PCys and PCys-s probes exhibited high selectivity and sensitivity toward H_2O_2 and GSH, respectively. The fluorescence intensity ratio of PCys to Cy5 was linearly correlated with the concentrations of H_2O_2 and GSH under various λ_{ex} (Supplementary Figs. 27–29). Consequently, the concentrations of these redox substances can be accurately determined using a standard curve. The detection limits for H_2O_2 and GSH were 5 and 2.5 μM, respectively, which are comparable to those of established probes for these substances[42–44]. This study introduces a non-conjugate polymer system that can switch its fluorescence in

https://doi.org/10.1038/s41467-024-54473-x

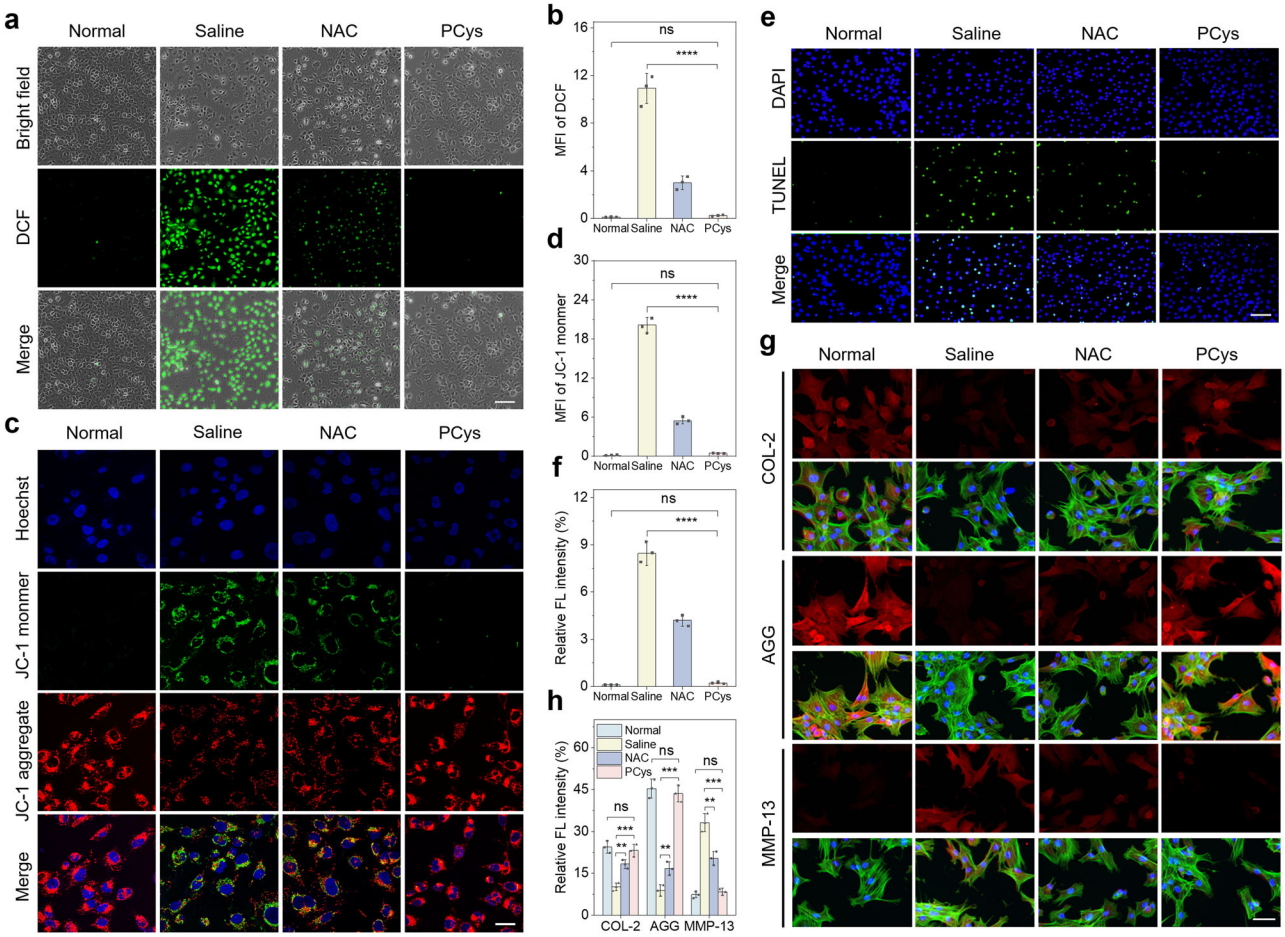

Fig. 4 | In vitro suppression of oxidative stress and protective effect of PCys on chondrocytes. a Intracellular ROS detection with DCFH-DA obtained by fluorescence microscope after treatments with saline, NAC, and PCys. Scale bars: 100 μm. **b** ImageJ analysis of DCFH-DA staining. **c** Mitochondrial membrane potentials of chondrocytes determined with JC-1 staining after treatments with saline, NAC, and PCys. Scale bars: 20 μm. **d** ImageJ analysis of JC-1 staining. **e** Fluorescence images of chondrocytes with TUNEL staining after treatments with saline, NAC, and PCys. Scale bars: 100 μm. **f** ImageJ analysis of TUNEL staining. **g** Immunofluorescence staining for COL-2, AGG and MMP-13 after treatments with saline, NAC, and PCys. Scale bars: 30 μm. **h** ImageJ analysis of immunofluorescence staining (left to right: $^{**}P = 0.0065$, $^{***}P = 0.0008$, $^{**}P = 0.0068$, $^{***}P = 0.0004$, $^{**}P = 0.0074$, $^{***}P = 0.0006$). Statistical significance: $^{**}P < 0.01$, $^{***}P < 0.001$, $^{****}P < 0.0001$. Data are presented as the mean with SD ($n = 3$ independent cells) in (**b**, **d**, **f** and **h**). Statistical differences were analyzed by a one-way ANOVA with Tukey's multiple comparisons test. ns means no significance. Each experiment was repeated three times independently with similar results.

response to redox changes and simultaneously quantify ROS and GSH with high accuracy.

Multicolor cell imaging and redox detection

To explore the potential of PCys in biomedical applications, we incubated the polymeric assemblies with 4T1 cancer cells and chondrocytes. The polymers did not show any inhibitory effect against the cells even at a high concentration (5 mg/mL) with 24 or 48 h of incubation (Supplementary Fig. 30). Owing to their intrinsic and excitation-dependent emission characteristics, PCys exhibited distinct intracellular fluorescence and outlined the cell contours clearly under different excitation wavelengths (405, 488 and 561 nm) (Fig. 3a), demonstrating their great potential for multicolor cell imaging. Taking advantage of the redox switchable fluorescence of PCys, we further measured the contents of H_2O_2 and GSH in 4T1 cells before and after incubation with H_2O_2 (1 mM) or GSH (5 mM) (Fig. 3b). Based on the standard curves established from ratiometric fluorescence probes, the H_2O_2 concentrations in 4T1 cells before and after H_2O_2 treatment were calculated to be 0.032 and 1.006 mM, respectively (Fig. 3c, d), while the intracellular GSH levels before and after incubation with GSH were determined to be 2.33 and 7.16 mM, respectively (Fig. 3e, f). The results are in good agreement with those obtained by commercial H_2O_2 and GSH assay kits, demonstrating the great potential of this nonclassical fluorescent polymer for detecting the intracellular redox microenvironment.

In vitro antioxidant and anti-inflammatory activity

PCys emerges as a promising candidate for the theragnosis of diseases associated with oxidative stress, owing to its antioxidative thiol groups and excellent fluorescence properties. To validate this potential, we chose chondrocytes as a model and induced an oxidative and inflammatory response via interleukin-1β (IL-1β) stimulation. Subsequently, the inflamed cells were treated with PCys, using a clinically established frontline antioxidant N-acetylcysteine (NAC) as a control. We first detected the intracellular ROS generation induced by IL-1β using 2′,7′-dichlorodihydrofluorescein diacetate (DCFH-DA) as a probe. DCFH-DA penetrates the cell membrane, undergoes intracellular esterase hydrolysis to form dichlorofluorescin (DCFH), which is subsequently oxidized by ROS to yield fluorescent dichloro-fluorescein (DCF)[45]. Notably, cells in the saline group exhibited intense green fluorescence, indicative of elevated ROS levels (Fig. 4a, b). Contrastingly, treatments with both NAC and PCys effectively alleviated cellular oxidative stress. Intriguingly, PCys demonstrated a markedly better antioxidative effect compared to NAC, despite equivalent thiol content. To explore this

https://doi.org/10.1038/s41467-024-54473-x

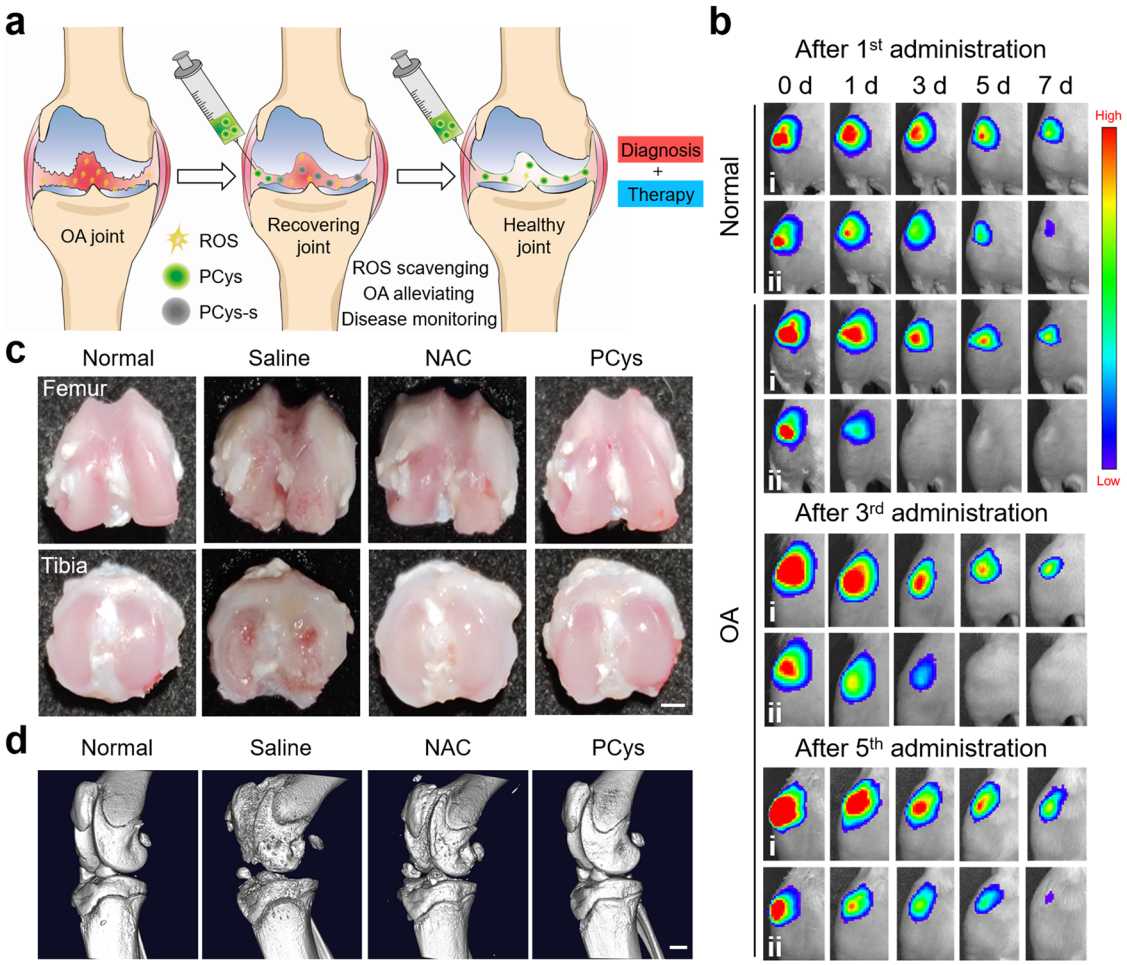

Fig. 5 | In vivo theranosis of OA. a Schematic illustration of PCys for bioimaging and theragnosis of OA in vivo. **b** IVIS imaging of rats with intra-articular injection of PCys-Cy5 for different times. i and ii represent the fluorescence of Cy5 and PCys, respectively. **c** Gross appearance evaluation of articular cartilage after various treatments. Scale bars: 1 mm. **d** Micro-CT 2D images of the knee joints of the rats after different treatments. Scale bars: 1 mm.

phenomenon, we conducted in vitro antioxidant analyzes using H_2O_2 and hydroxyl radical (·OH) as representative ROS. We found that PCys scavenged these ROS more rapidly and efficiently than NAC (Supplementary Fig. 31). This enhanced efficacy can be attributed to the hierarchical structure of the polymer, which likely promoted the interactions between thiol groups and ROS or facilitated a synergistic effect among the thiol groups[46,47].

Oxidative stress is a well-documented inducer of apoptosis and disruptor of mitochondrial membrane integrity[48]. This mitochondrial dysfunction within apoptotic chondrocytes further escalates the production of ROS. Consequently, we assessed the effect of antioxidant therapy on mitochondrial membrane potential, a primary indicator of early apoptosis[49], using JC-1 staining. Under normal conditions, mitochondria exhibit high membrane potential, manifested as red fluorescence. In contrast, our observations revealed that inflamed cells showed abundant green fluorescence, reflecting severe mitochondrial damage (Fig. 4c, d). NAC treatment resulted in a reduction in green fluorescence intensity, suggesting an alleviation of mitochondrial damage. Impressively, PCys treatment nearly eradicated green fluorescence, indicating minimal mitochondrial impairment. We also evaluated cellular apoptosis using terminal deoxynucleotidyl transferase-mediated dUTP nick-end labeled (TUNEL) assay and flow cytometry (Fig. 4e, f and Supplementary Fig. 32). It was found that both PCys and NAC effectively hindered oxidative stress-induced cell death. Notably, PCys exhibited a significantly lower apoptosis rate (5.8%) than the NAC (16%) and saline-treated group (28.7%). Furthermore, we investigated the expression of cartilage phenotype and inflammatory markers to assess the progression of inflammation. This included an analysis of cartilage catabolic inflammatory genes (tumor necrosis factor-α (TNF-α), interleukin-6 (IL-6), cyclooxygenase-2 (COX-2), matrix metalloproteinases-13 (MMP-13) and thrombospondin motifs-5 (ADAMTS-5)) and chondrogenic markers genes (cartilage-specific genes collagen type-2 (COL-2), aggrecan (AGG) and sry-type high-mobility-group box 9 (SOX-9)) through quantitative reverse transcription polymerase chain reaction (qRT-PCR) and immunofluorescence techniques (Fig. 4g, h and Supplementary Fig. 33). The results revealed that oxidative stress led to an upregulation of inflammatory genes and a downregulation of osteogenic genes, thereby exacerbating inflammation. Notably, PCys treatment normalized the expression of these genes to levels comparable to those of the normal group, demonstrating its potent efficacy in suppressing that oxidative stress-induced inflammation.

In vivo theranostics of osteoarthritis

Antioxidant plays a key role in the early intervention of OA, yet commonly used small molecule drugs such as NAC are limited by rapid metabolism and the need for frequent administration. This not only poses the risk of toxic side effects, but also adversely affects patient compliance[50]. In this context, PCys showed not only enhanced antioxidative, anti-inflammatory, and anti-apoptotic activities but also a linear fluorescence response to the redox microenvironment, rendering it a promising candidate for both OA treatment and real-time

https://doi.org/10.1038/s41467-024-54473-x

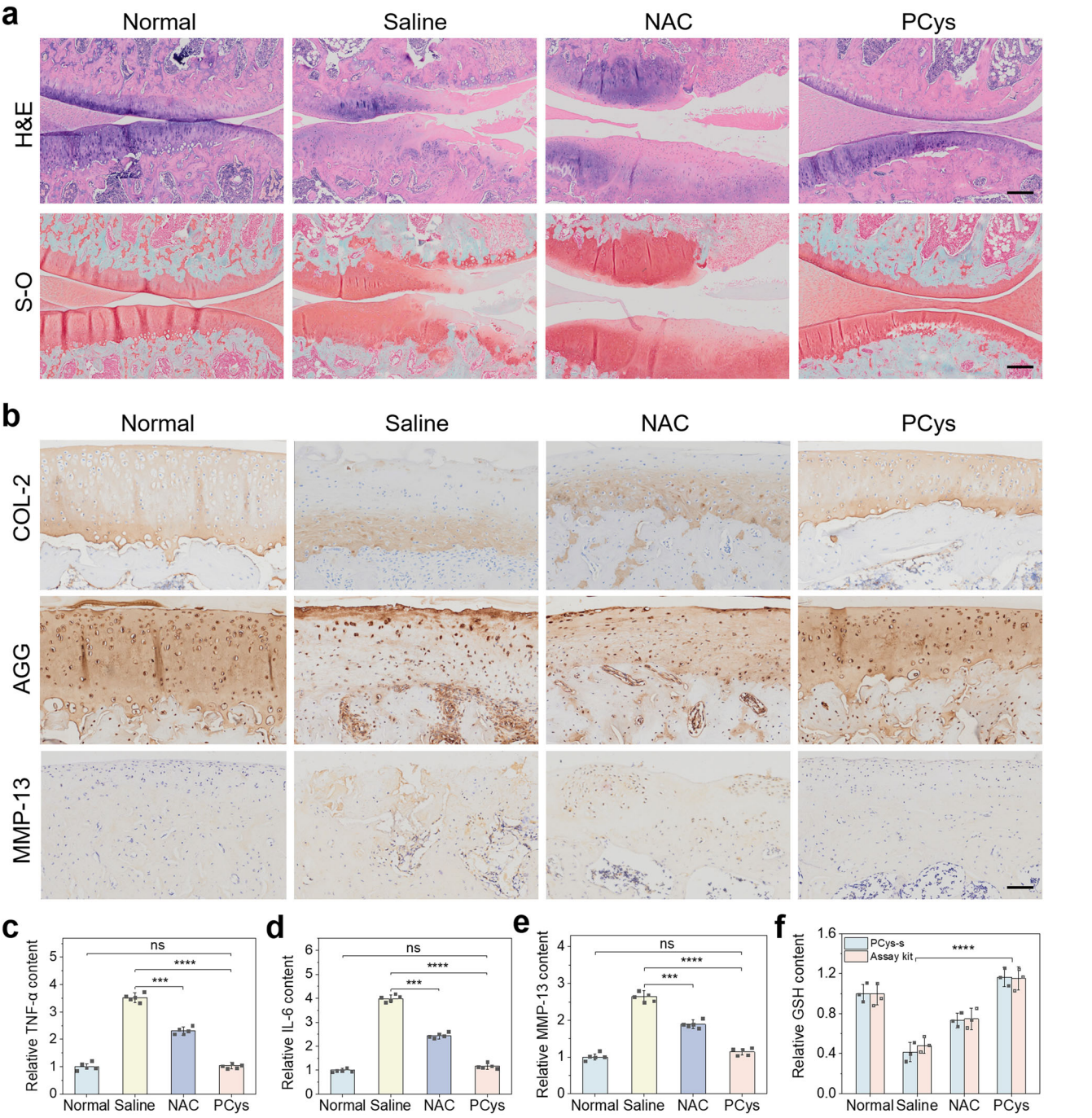

Fig. 6 | Histopathological and immunohistochemical analysis. a H&E and safranin O/fast green staining of rat OA knee joints after different treatments. Scale bars: 200 μm. Each experiment was repeated three times independently with similar results. **b** Immunohistochemical staining of COL-2, AGG and MMP13. Scale bars: 200 μm. Each experiment was repeated three times independently with similar results. **c**–**f** The levels of TNF-α (**c**, ***$P = 0.0008$), IL-6 (**d** ***$P = 0.0007$), MMP-13 (**e** ***$P = 0.0009$), and GSH (**f**) in the synovial fluid after different treatments. Statistical significance: ***$P < 0.001$, ****$P < 0.0001$. Data are presented as the mean with SD ($n = 5$) independent samples in (**c**–**e**) $n = 3$ independent samples in (**f**). Statistical differences were analyzed by a one-way ANOVA with Tukey's multiple comparisons test. ns means no significance.

disease progression monitoring (Fig. 5a). To study the retention of the polymer in the joint cavity, we first injected Cy5-labeled PCys and free Cy5 dye into the joint cavity of healthy rats. In vivo imaging revealed that the fluorescence from free Cy5 almost vanished within 2 d, while the polymer-treated group maintained strong Cy5 fluorescence after 7 d, indicating prolonged persistence of the macromolecule in the joint cavity (Supplementary Fig. 34). This property has the potential to improve the efficacy and longevity of OA therapy, thereby reducing the frequency of drug administration. Furthermore, to evaluate the utility of PCys in OA theragnosis, we established an OA rat model by intra-articular injection of monosodium iodoacetate (MIA). The rats received various treatments at 0, 7, 14, 21, and 28 d. In healthy rats, the fluorescence of PCys was sustained for over 7 d (Fig. 5b). In contrast, in the OA group, PCys fluorescence was rapidly quenched and became undetectable within 2 d (Fig. 5b), due to the oxidation of thiol groups by elevated levels of ROS present in the synovial fluid. This finding confirmed the successful establishment of the OA model and underscored the sensitivity of PCys to the oxidative environment

characteristic of OA pathology. As treatment progressed and oxidative stress diminished, PCys fluorescence gradually recovered. After five treatments, the reduced ROS levels in the synovial fluid allowed the fluorescence of PCys to persist for an extended duration, similar to that observed in healthy joints (lasting beyond 7 d). In addition, ROS concentration in the synovial fluid was estimated to be ~10.2 μM using the ratiometric fluorescent probe (Supplementary Fig. 35), which is similar to that in normal rats (~8 μM)[51]. The result indicates that PCys not only effectively treated OA but also enabled real-time monitoring of ROS levels in the joint cavity. The rats were then euthanized and the femur and tibia were examined macroscopically (Fig. 5c). The saline group showed severe erosion of the femur and tibia, and the NAC group had some therapeutic effects but still exhibited minor erosion. The articular surface was irregular and extensively eroded in the saline and NAC-treated OA groups. In contrast, the normal and PCys groups had smooth and glossy articular surfaces. Further micro computed tomography (Micro-CT) imaging confirmed significant bone destruction and osteophyte formation in the saline group, while the PCys group more effectively prevented OA progression and cartilage degradation compared with other groups (Fig. 5d).

The decalcified tissue specimens were sectioned and stained to evaluate the therapeutic effects of PCys by histological assessment (Fig. 6a). The H&E staining revealed that the normal group had orderly and compact chondrocytes, with smooth and intact articular cartilage surface, while the saline group displayed typical OA features, such as surface disruption, erosion, fissures and evident chondrocyte degeneration or necrosis. PCys treatment could markedly inhibit cartilage damage, with abundant bone marrow cells in the bone marrow cavity and normal morphology of the articular cartilage matrix. Safranin-O (S-O) staining was conducted to examine extracellular cartilage matrix (ECM) changes. It was found that PCys treatment could enhance the expression of proteoglycans in articular cartilage. Further immunohistochemical analysis indicated that the expression levels of COL-2 and AGG were the highest in the PCys group, while the expression level of MMP-13 was reduced, suggesting that PCys could better protect the ECM from degradation (Fig. 6b). In addition, enzyme-linked immunosorbent assay (ELISA) kits were used to measure the expression levels of TNF-α, IL-6 and MMP-13 in the synovial fluid (Fig. 6c–e). The results indicated that PCys could significantly decrease the expression of these pro-inflammatory factors in vivo, alleviating the inflammation caused by OA.

To investigate the therapeutic mechanism of PCys, we used PCys-s as a reducing probe to measure the GSH content in the synovial fluid of different treatment groups (Fig. 6f). Interestingly, we found that the GSH concentration in the synovial fluid of the PCys group was even higher than that of the normal group. The same conclusion was also confirmed by using a commercial GSH detection kit, which further validated the accuracy of PCys-s for detecting reductive substances in vivo. The results suggest that the antioxidant mechanism of PCys involves not only the thiol-mediated depletion of ROS (direct antioxidant) but also the stimulation of GSH production (indirect antioxidant). This dual mechanism is similar to that of NAC since the degradation product of PCys, L-cysteine, can be utilized for GSH synthesis in vivo[52–54]. It is worth noting that the GSH content in the synovial fluid of the PCys group was slightly higher than that of the normal group. This may be because the process of GSH generation in the joint was still ongoing at the time of sampling. The lower GSH content in the NAC group was mainly attributed to its shorter retention time in the joint cavity and lower ROS scavenging ability. Finally, the H&E staining analysis of the main organs did not show any abnormality, indicating excellent biocompatibility of PCys (Supplementary Fig. 36). Therefore, PCys, as a polymer material with bioactivity and biocompatibility, demonstrates better therapeutic effects for OA compared to first-line clinical antioxidants. Additionally, it possesses dynamic fluorescence imaging capabilities that traditional drugs lack, highlighting its great potential for the theragnosis of ROS-related diseases such as cancer, inflammatory, and degenerative diseases. Ongoing studies in our laboratory are further exploring these applications.

Discussion

In conclusion, we report a non-classical luminescent aliphatic polymer utilizing aggregated thiols as chromophores. The polymer showed molecular weight-dependent high QY, excellent multicolor luminescence and imaging properties. Moreover, the fluorescence of the polymer could be reversibly switched off and on under oxidative and reductive conditions, respectively, enabling quantitative detection of ROS and GSH in cells and in vivo. In addition, the bioactive polymer demonstrated greater and more enduring antioxidant properties compared to first-line clinical antioxidants, enabling long-term treatment and diagnosis of OA. This fluorescent polymer featured a simple structure, good biocompatibility, a distinctive luminescence mechanism, and numerous active sites for functionalization. It is expected to advance bioactive imaging materials with potential for clinical translation in biosensing, drug delivery, and disease theragnosis applications.

Methods

Ethical regulations

The research presented here complies with all relevant ethical regulations. All experiments involving animals were reviewed and approved (20220711001) by the institutional ethics committee of West China Hospital, Sichuan University.

Materials

Methoxypolyethylene glycol amine (MPEG-NH_2, MW 5000) was purchased from Suzhou Nords Parson's Pharmaceutical Technology Co., Ltd. (Suzhou, China). L-cysteine (99%), benzyl chloroformate (98%) and triphosgene (99%) were obtained from Aladdin. Fluorescein isothiocyanate isomer I (FITC, 90%) was obtained from Acros Organics (New Jersey, USA). Glutathione (GSH) was purchased from Biofroxx (Einhausen, German). 2,7-Dichlorodihydrofluorescein diacetate (DCFH-DA) and 3, 3′, 5, 5′-tetramethylbenzidine (TMB) were obtained from Adamas Reagent, Ltd. (Shanghai, China). Cell counting kit-8 (CCK-8) was purchased from Beijing Labgic Technology Co., Ltd. (Beijing, China). 5,5′-Dithiobis-(2-nitrobenzoic acid) (DTNB) was acquired from Shanghai Haohong Scientific Co., Ltd. (Shanghai, China). 3,3′-Diethylthiadicarbocyanine iodide (Cy5) was obtained from Alfa Aesar (China) Chemistry Co., Ltd. (Shanghai, China). H_2O_2 (30 vol.%) was purchased from Chengdu JinShan Chemical Regent Co., Ltd. (Chengdu, China). Tetrahxydrofuran (THF) and *n*-hexane were attained from General-Reagent and purified by refluxing with sodium wire and benzophenone under nitrogen, followed by fractional distillation. *N*,*N*-Dimethylformamide (DMF) was purchased from General-Reagent and dried over CaH_2 (5% w/w), then distilled at 20 mm Hg and stored over 4 A molecular sieves. All other reagents were used as received from commercial sources.

Characterization

cProton nuclear magnetic resonance spectroscopy (^{1}H NMR, 400 MHz) was recorded on a Bruker Avance III HD spectrometer using tetramethylsilane (TMS) as an internal standard and CF_3COOD or DMSO-d_6 as solvent at room temperature. Fourier transform infrared (FTIR) spectroscopy was recorded from 4000 to 500 cm^{-1} using a Nicolet iS10 spectrometer (Thermo Electron Corporation, U.S.A). Gel permeation chromatography (GPC) was carried out on an HLC-8320 (TOSOH Corporation, Japan) at room temperature using DMF/LiBr (2 g L^{-1}) as an eluent. Fluorescence measurement was conducted on an F-4600 FL spectrophotometer (Hitachi, Ltd., Japan). UV-vis absorbance spectra were obtained using a UV2600 spectrophotometer

(Techcomp, Ltd., China). Dynamic light scattering (DLS) was performed on a Malvern nano-zeta sizer instrument (Malvern Instruments Ltd., UK) at room temperature at an angle of 90°. Transmission electron microscopy (TEM) was performed on model H-600-4 (Hitachi, Ltd., Japan) with an accelerating voltage of 75 kV. The Image J software was used to measure the fluorescence intensity of images.

Synthesis of S-carbobenzoxy-L-cysteine (L-Cys-Cbz)

L-Cysteine (12.12 g) was dissolved in 120 mL of ice-cooled ether containing triethylamine. To this solution, benzyl chloroformate (17.2 g) in 200 mL of ether was added dropwise added with vigorous stirring. The reaction mixture was stirred at 0 °C for 1 h and then at room temperature for 12 h. The precipitation was filtered, washed with ethanol, acetone, and ether in sequence, and dried under vacuum to afford L-Cys-Cbz as a white powder (74% yield).

Synthesis of S-carbobenzoxy-L-cysteine-*N*-carboxyanhydride (L-Cys-Cbz NCA)

L-Cys-Cbz (10.0 g) was dissolved in dry THF (140 mL) in a Schlenk flask and treated with triphosgene (4.5 g) in anhydrous THF (60 mL) dropwise under argon. The mixture was stirred under argon at 50 °C for 4 h. The resulting clear solution was concentrated under reduced pressure and recrystallized from dry THF/*n*-hexane three times. The obtained product was dried under a vacuum to provide L-Cys-Cbz NCA as a white powder (72% yield).

Synthesis of MPEG-PCys-Cbz

MPEG-PCys-Cbz was synthesized by ring opening polymerization of L-Cys-Cbz NCA initiated by MPEG-NH_2 according to previous reports[19]. Briefly, L-Cys-Cbz NCA (0.31, 0.51, 2.04, 3.06, and 4.08 g) was dissolved in anhydrous DMF (20 mL) in a Schlenk tube. Then MPEG-NH_2 (2.0 g) in anhydrous DMF (5 mL) was added and the reaction was carried out for 3 d at 37 °C under argon. The product was isolated by precipitation in ice-cold diethyl ether three times and obtained as a pale-yellow solid (72% yield).

Synthesis of MPEG-PCys (PCys$_x$)

MPEG-PCys-Cbz (2.0 g) was dissolved in 20 mL of CF_3COOH in a Schlenk tube and treated with an appropriate amount of 33% HBr. The mixture was stirred at 0 °C for 2 h and the volatiles were removed under reduced pressure using a rotary evaporator. The residue was coevaporated with small volumes of CH_2Cl_2 several times to remove TFA and HBr. The mixture was precipitated in ice-cold diethyl ether three times to give a pale-yellow solid (81% yield).

Self-assembly of copolymers

PCys$_x$ assemblies were prepared by a dialysis method[15]. In brief, PCys (10 mg) in 1 mL of DMF was added dropwise to 9 mL of deionized water with rapid stirring. The resulting solution was transferred to a dialysis bag (MWCO 3500) and dialyzed against deionized water for 3 d, changing the water every 4 h. Finally, the solution was centrifugalized for 15 min at 861 xg and filtered through a 0.45 μm pore-sized syringe filter (Millipore, Carrigtwohill, Co. Cork, Ireland).

Determination of free thiol group content

The content of thiol groups was determined by 5,5-dithio-bis-(2-nitrobenzoic acid) (DTNB, Ellman's reagent). DTNB was dissolved in 0.1 M sodium phosphate buffer (pH 8.0) containing 1 mM EDTA at a concentration of 100 μg mL^{-1}. PCys in H_2O or DMF was added to the same buffer at a concentration of 2.5 mg mL^{-1}. Then 20 μL of the PCys solution was mixed with 180 μL of the DTNB solution in a microplate and incubated for 15 min at room temperature. The absorbance was measured at 412 nm using a microplate reader (DNM-9602, Nanjing Perlove Medical Equipment Co., Ltd., China). A cysteine standard curve was used to calculate the content of free thiols in the polymer.

Fluorescence quantum yield (QY) measurement

The QYs of PCys in H_2O were measured in reference to quinine sulfate in 0.1 M H_2SO_4 (literature quantum yield 54% at 350 nm excitation)[29]. The same excitation wavelength and slit band widths were applied for the two samples. The formula used for QY measurements was as follows.

$$QY = (I/I_R) \times (A_R/A) \times (\eta/\eta_R)^2 \times QY_R \quad (1)$$

where QY is the quantum yield of the sample, I is the integral area under the fluorescence spectrum, η is the refractive index of the solvent used, and A is the absorbance at the excitation wavelength. The subscript R represents the reference. To minimize reabsorption effects, absorbencies were kept under 0.05 at the excitation wavelength of 350 nm.

AIE properties of PCys

Fluorescence spectra (λ_{ex} = 370 nm) of PCys in DMF-ether mixtures (0.04 mg mL^{-1}) with varying ether fractions (f_{Et}) were recorded on an F-4600 FL spectrophotometer (Hitachi, Ltd., Japan) at 25 °C, using an emission slit width of 5 nm and constant scan rate.

Fluorescence resonance energy transfer (FRET) study

Samples for the FRET studies were prepared by adding appropriate concentration of FITC (receptor) in deionized water (0.2 mL) to 2 mL PCys assemblies (donor, 1 mg mL^{-1}) with constant stirring for 1 h, and then ultrasonated for 2 h. the aqueous solution was transferred to a dialysis bag (MWCO 3500) and dialyzed against water for 24 h, changing the water every 3 h. Then, the donor was excited at 370 nm and the emission spectra were recorded on an F-4600 FL spectrophotometer (Hitachi, Ltd., Japan).

Film preparation

The polymer film was prepared by a solution casting method as follows. A copolymer solution (5 mg mL^{-1} in DMF) was cast onto glass plates and dried at 50 °C until the solvent was completely evaporated. The resulting film was peeled off from the glass plates and vacuum-dried at room temperature for 24 h before characterization.

Fluorescence stability of PCys

PCys assemblies and PCys dissolved in DMF were exposed to air at 25 °C with continuous stirring. The fluorescence spectra of PCys in H_2O (λ_{ex} = 370 nm) and DMF (λ_{ex} = 330 nm) were recorded at various time intervals using an F-4600 FL spectrophotometer (Hitachi, Ltd., Japan), all measurements were conducted at 25 °C.

Responsiveness of PCys and PCys-s

Both PCys and PCys-s in H_2O or DMF (2 mg mL^{-1}) were treated with different concentrations of H_2O_2 and GSH, respectively. The fluorescence intensity of the samples over time was monitored using an F-4600 FL spectrophotometer (Hitachi, Ltd., Japan) with λ_{ex} of 370 nm for H_2O and 330 nm for DMF. To investigate the reversibility of fluorescence, the fluorescence intensity of PCys assemblies after treatment with H_2O_2 and GSH was repeatedly measured. The addition of H_2O_2 and GSH was conducted multiple times for the measurements.

Theoretical calculation study

The fluorescence mechanism of PCys was elucidated through time-dependent density functional theory (TD-DFT), with calculations were performed using the ORCA 4.0.0.2 program package. The computations were carried out at the B3LYP/6-31 G(d) level of theory.

Extracellular H_2O_2 scavenging activity

The H_2O_2 scavenging capacity of PCys was measured by the Hydrogen Peroxide Detection Kit (NanJing JianCheng Bio Inst, Nanjing, China).

H_2O_2 reacts with ammonium molybdate to form a yellow complex with an absorbance peak at 405 nm. PCys (1 mg mL^{-1}) was incubated with 2 mM H_2O_2 at 37 °C for 2 h. After the reaction, the concentration of the remaining H_2O_2 was determined according to the manufacturer's instructions and the H_2O_2-eliminating capacity was calculated. NAC (0.48 mg mL^{-1}) was used as a positive control and tested by the same method.

Extracellular hydroxyl radical (·OH) scavenging activity

The ·OH scavenging activity of PCys was evaluated by the TMB chromogenic method[55]. OH was generated by the Fenton reaction between H_2O_2 and Fe^{2+}, which can oxidize TMB to oxTMB with a characteristic absorption at 652 nm. The concentration of the remaining ·OH can be determined by monitoring the absorption of oxTMB at 652 nm. In detail, the test solutions containing 250 μM TMB, 2 mM H_2O_2, 1 mM $FeSO_4$ and PCys (1 mg mL^{-1}) in HAc/NaAc buffer (0.5 M, pH 4.5) were prepared in the dark and rested for 5 min. Then the absorbance peak at 652 nm of the solution was measured with a UV-vis spectrophotometer. NAC (0.48 mg mL^{-1}) was used as a positive control and tested by the same method.

Cell lines

4T1 cells and chondrocytes were selected for cellular assays. The 4T1 cells, obtained from the Shanghai Institute of Biochemistry and Cell Biology, Chinese Academy of Sciences, were first cultured in Dulbecco's Modified Eagle's Medium (DMEM) supplemented with 10% heat-inactivated fetal bovine serum (FBS, GIBCO), 100 units per mL of penicillin, and 100 units per mL of streptomycin (Sigma). This culture was maintained in a 5% CO_2 atmosphere at 37 °C. Chondrocytes were isolated from rat cartilage. The cartilage was first treated with a 0.25% trypsin solution for 30 min, followed by a 12-h digestion in a 0.1% collagenase II solution. Post-digestion, the chondrocytes were harvested and subsequently cultured in DMEM supplemented with 10% fetal bovine serum (FBS), under the same conditions of temperature and CO_2 concentration as the 4T1 cells.

Cell viability

4T1 cells and chondrocytes were seeded in 96-well plates at a density of 5000 cells per well. Following a 24-h incubation, the media was discarded, and a serial of different concentrations of PCys were introduced into fresh RPMI 1640 complete medium and added to the wells. After incubation periods of 24 or 48 h, the cells were washed three times with PBS. Subsequently, 100 μL of fresh media containing 1 mg mL^{-1} of CCK-8 (Dojindo, Japan) was dispensed into each well. The absorbance at 490 nm was measured using a microplate reader. Cell viability as calculated using the formula:

$$\text{Cell viability}(\%) = (OD_{490nm}\text{of the sample}/OD_{490nm}\text{of the control}) \times 100\%$$

Multicolor cell imaging

4T1 cells and chondrocytes (both 1×10^5) were plated on coverslips in six-well plates. After 24 h, the cells were treated with 200 μg mL^{-1} of PCys for 4 h. Then, the cells were washed with PBS three times and fixed with 4% formaldehyde for 30 min. Finally, the cells were imaged on a CLSM under various channels (Olympus FV1000, Japan). Conditions: λ_{ex} = 405 nm, λ_{em} = 410-750 nm; λ_{ex} = 488 nm, λ_{em} = 515-750 nm; λ_{ex} = 561 nm, λ_{em} = 575-750 nm.

Intracellular ROS detection

Chondrocytes (1×10^5) were plated on coverslips in six-well plates. After 24 h, the cells were exposed to different concentrations of H_2O_2 (0 and 1 mM) for 60 min. Then, the cells were treated with 1 mg mL^{-1} of PCys-Cy5 for 2 h. Afterwards, the cells were washed with PBS three times and fixed with 4% formaldehyde for 30 min. Finally, the cells were observed on a CLSM under various channels (Olympus FV1000, Nikon A1RMP, Japan). Moreover, the ROS levels in the cell homogenate were examined by using H_2O_2 assay kits (NanJing JianCheng Bio Inst, Nanjing, China),

Intracellular GSH detection

Chondrocytes (1×10^5) were plated on coverslips in six-well plates. After 24 h, the cells were treated with different concentrations of GSH (0 and 5 mM) for 60 min. Then, the cells were incubated with 1 mg mL^{-1} of PCys-s-Cy5 for 2 h. Next, the cells were washed with PBS three times and fixed with 4% formaldehyde for 30 min. Finally, the cells were imaged on a CLSM under various channels (Olympus FV1000, Nikon A1RMP, Japan). In addition, the GSH levels in the cell homogenate were determined by using GSH assay kits (NanJing JianCheng Bio Inst, Nanjing, China), following the manufacturer's instructions.

Cell apoptosis assay

Cell apoptosis was evaluated using the Annexin V-FITC/PI apoptosis detection kit and TUNEL staining analysis. Chondrocytes (1×10^5) were seeded in six-well plates and subjected to treatments with or without 10 ng mL^{-1} IL-1β, in conjunction with NAC and PCys. After 24 h of incubation, cells were washed and resuspended in Binding Buffer containing Annexin V-FITC and PI (KeyGEN, China). Flow cytometry (BD Biosciences, USA) was employed for the detection of apoptotic cells. For TUNEL staining, cells were processed using an apoptosis detection kit (Roche), adhering to the manufacturer's protocol. Briefly, after 24 h of incubation, cells were washed and fixed with 4% paraformaldehyde for 20 min at room temperature, followed by permeabilization with 0.1% Triton X-100. After fixation in proteinase K for 15 min, cells were stained with the TUNEL mixture for 60 min, incubated with DAPI for 5 min, and visualized using fluorescence microscopy.

Intracellular ROS scavenging activity

Chondrocytes (1×10^5) were seeded in six-well plates and treated with or without 10 ng mL^{-1} IL-1β, along with NAC and PCys in different groups. After 48 h, the cells were washed three times with PBS and incubated for 20 min with serum-free DMEM containing 2′,7′-dichlorodihydrofluorescein diacetate (DCFH-DA, Beyotime, China). The intracellular green fluorescence intensity was measured at λ_{ex}/λ_{em} = 488/525 nm and then imaged and analyzed using ImageJ software.

Mitochondrial membrane potential determination

Mitochondrial membrane potential was evaluated in chondrocytes using JC-1 staining. Chondrocytes (1×10^5) were plated in six-well plates and subjected to treatments with or without 10 ng mL^{-1} IL-1β, alongside NAC and PCys in different experimental groups. Following treatments, chondrocytes were harvested and incubated with JC-1 (5 μg mL^{-1}) for 25 min at 37 °C. After staining, cells were washed thrice with PBS to eliminate excess JC-1. Flow cytometry analysis was conducted using a BD Accuri C6 plus flow cytometer.

Quantitative real-time polymerase chain reaction (RT-qPCR) analysis

Chondrocytes (1×10^5) were cultured in six-well plates and subjected to treatments with or without 10 ng mL^{-1} IL-1β, in combination with NAC and PCys, across various groups. The gene expressions of TNF-α, IL-6, COX-2, ADAMTS5, MMP-13, SOX-9, COL-2, and AGG were analyzed using RT-qPCR. The total RNA isolated from the cells employing TRIzol reagent (Invitrogen, USA) according to the manufacturer's protocol. To minimize randomization error, each gene expression analysis was performed in triplicate.

Immunofluorescence

The expression of OA catabolic biomarkers MMP-13 and chondrogenic markers genes (COL-2 and AGG) in chondrocytes was assessed by immunofluorescence. Chondrocytes were seeded onto sterile glass coverslips in 24-well plates at a density of 2×10^5 cells per well, treated with IL-1β, and incubated with saline, NAC and PCys for 12 h. The cells were washed with PBS, fixed in 4% paraformaldehyde for 10 min, treated with 0.1% Triton X-100 for 15 min, and incubated in 3% bovine serum albumin/PBS for 30 min at room temperature. Subsequently, the cells were washed with PBS and incubated with primary antibody as follows: MMP-13 (Life Tech, USA, 1:200 dilution), COL-2 (Life Tech, USA, 1:200 dilution) and AGG (Life Tech, USA, 1:200 dilution) at 4 °C overnight. After incubation, the cells were washed with PBS again and incubated with appropriate Alexa Fluor conjugated secondary antibodies (Molecular Probes, Life Tech, USA, 1:400 dilution) at room temperature for 1 h. The 4, 6-diamidino-2-phenyindole dilactate (DAPI, Life Tech, USA) and Alexa Fluor 594 phalloidin (Life Tech, USA) were used to counterstain cellular nuclei and actin rings, respectively. The immunofluorescence images were acquired by using the laser scanning confocal microscopy. The protein expression levels of MMP-13, COL-2 and AGG were also acquired based on the fluorescence intensity of the images for quantitative comparison using Image J software.

OA model and in vivo therapy

The male *Sprague Dawley* rats (6-8 weeks old) were obtained from Vital River Company (Beijing, China) and treated according to the standard guidelines approved by the institutional ethics committee of West China Hospital, Sichuan University. The rats were anesthetized by intraperitoneal injection of 0.5% sodium pentobarbital (10 mL kg^{-1}) before each intervention. OA was induced by a single intra-articular injection of MIA (50 µL, 30 mg mL^{-1}; Sigma-Aldrich) into the right knee joint through the infrapatellar ligament. The left knee joint received an equal volume of saline as a control. Three weeks after MIA injection, the rats were randomly divided into three groups ($n = 5$) and treated with intra-articular injections of saline, NAC (50 mg mL^{-1}), or PCys (104 mg mL^{-1}) into the right knee joint. The thiol content of NAC and PCys was equivalent and corresponded to the typical clinical dose. The treatment was repeated every seven days for a total of five times. The first day of treatment was designed as day 0. Five weeks after the initial MIA injection, the rats were euthanized by an overdose anesthesia and the knee joints were collected for further analysis.

IVIS imaging

To evaluate the retention of the injected materials in the knee joint, six OA rats were randomly assigned to two groups ($n = 3$) and anesthetized with isoflurane. The rats received an intra-articular injection of Cy5 or PCys-Cy5 in saline solution. The rats were then imaged by an in vivo imaging system (IVIS) at an excitation wavelength of 640 nm and emission wavelength of 680 nm at different time points.

Similarly, three normal rats and five OA rats were anesthetized with isoflurane and injected with PCys-Cy5 solution intra-articularly. The rats were imaged by IVIS at excitation wavelength of 480 nm or 640 nm and emission wavelength of 520 nm or 680 nm, respectively, at various time points.

Macroscopic observation

After carefully removing the muscles, ligaments, and meniscal tissues around the knee joint, the femoral condyle was separated from the tibial plateau, and the gross appearance of articular cartilage was evaluated under direct visualization.

Micro-CT arthrography

The rats were euthanized at 5 weeks, and the knee joint samples were collected for arthrography using a high-resolution micro-CT imaging system (SkyScan 1172, Bruker BioSpin, Belgium). The relative osteophytes volume was quantified based on the micro-CT scanning and reconstruction results.

H&E and Safranin-O staining

The extent of cartilage degeneration was assessed by hematoxylin-eosin (H&E) staining and Safranin-O staining. For H&E staining, the sections were immersed in hematoxylin solution for 5 min, washed running water and 95% alcohol, and then counterstained with 1% Eosin Y solution for 3 min. For Safranin-O staining, which specifically detects proteoglycan in cartilage, the sections were stained with Weigert's hematoxylin working solution for 10 min, followed by fast green solution for 5 min and 1% acetic acid. The sections were then stained with 0.1% Safranin-O solution for 5 min. The slides were examined under an Olympus DP70 inverted microscope (Japan) to evaluate the inflammation and cartilage degeneration.

Immunohistochemistry analysis

For immunohistochemical staining and immunofluorescent analysis, the sections were deparaffinized, rehydrated and blocked with 2% bovine serum albumin (BSA) containing 0.1% Triton X-100 for 1 h at room temperature. The sections were then incubated overnight at 4 °C with primary antibodies against COL-2, AGG and MMP13, followed by FITC-conjugated anti-rat secondary antibody (Ybscience, China, 1:100 dilution) for 1.5 h at room temperature in the dark. The sections were rinsed three times with PBS and stained with 4,6-diamidino-2-phenylindole (DAPI) for 10 min. Fluorescence images were obtained with a microscope and analyzed with Image-Pro Plus software, version 6.0 (Media Cybernetics, Inc., Rockville, USA).

Measurement of TNF-α, IL-6 and MMP-13 level in synovial fluid

Inflammatory markers within the synovial fluid, including TNF-α, IL-6, and MMP-13, were quantified by an enzyme-linked immunosorbent assay (ELISA) with a commercial ELISA kit (NanJing JianCheng Bio Inst, Nanjing, China) according to the instructions provided by the manufacturer. Absorbance was measured at a wavelength of 450 nm using a plate reader (Thermo Fisher, USA).

Measurement of GSH level in synovial fluid

The GSH levels within joint synovial fluid were determined by an enzyme-linked immunosorbent assay (ELISA) using a commercial ELISA kit (NanJing JianCheng Bio Inst, Nanjing, China) according to the instructions provided by the manufacturer. Absorbance readings were taken at a wavelength of 450 nm using a plate reader (Thermo Fisher, USA). In addition, GSH concentrations in the synovial fluid were determined using PCys-s-Cy5.

Histological studies

The biological safety of the treatment in vivo was assessed through H&E staining. Major organs (heart, liver, spleen, lung, and kidney) were harvested from rats post-treatments. The collected organs were fixed in 10% paraformaldehyde, embedded in paraffin, sectioned into slices ~4 µm thick, and stained with H&E. Fluorescence microscopy was utilized to observe and assess histopathological alterations.

Statistical analysis

The quantitative data were presented as means ± standard deviations (SD). Statistical analysis was performed using IBM SPSS statistics software, Version 19 (IBM, New York, USA). Student's t-test or one-way analysis of variance (ANOVA) was used to assess the statistical significance of the data at 95% confidence levels ($P < 0.0001$).

Reporting summary

Further information on research design is available in the Nature Portfolio Reporting Summary linked to this article.

Data availability

The raw data generated in this study are provided in the Supplementary Information/Source Data file. Source data are provided with this paper.

References

1. Paige, J. S., Wu, K. Y. & Jaffrey, S. R. RNA mimics of green fluorescent protein. *Science* **333**, 642–646 (2011).
2. Misteli, T. & Spector, D. L. Applications of the green fluorescent protein in cell biology and biotechnology. *Nat. Biotechnol.* **15**, 961–964 (1997).
3. Pédelacq, J. D. et al. Engineering and characterization of a superfolder green fluorescent protein. *Nat. Biotechnol.* **24**, 79–88 (2005).
4. Chen, T. T. et al. Fluorescence activation imaging of cytochrome c released from mitochondria using aptameric nanosensor. *J. Am. Chem. Soc.* **137**, 982–989 (2015).
5. Bhivotovsky, B. et al. Injected cytochrome c induces apoptosis. *Nature* **391**, 449–450 (1998).
6. Li, H. et al. Cytochrome c release and apoptosis induced by mitochondrial targeting of nuclear orphan receptor TR3. *Science* **289**, 1159–1164 (2000).
7. Rong, L. et al. A two-photon excitation based fluorogenic probe for sialome imaging in living systems. *Adv. Sci.* **3**, 1500211 (2015).
8. Mao, L. et al. Two-photon fluorescence imaging and specifically biosensing of norepinephrine on a 100-ms timescale. *Nat. Commun.* **14**, 1419 (2023).
9. Yang, J. et al. The influence of the molecular packing on the room temperature phosphorescence of purely organic luminogens. *Nat. Commun.* **9**, 840 (2018).
10. Li, J. et al. Supramolecular materials based on AIE luminogens (AIEgens): construction and applications. *Chem. Soc. Rev.* **49**, 1144–1172 (2020).
11. Li, X. et al. Visible-light-driven photoswitchable fluorescent polymers for photorewritable pattern, anti-counterfeiting, and information encryption. *Adv. Funct. Mater.* **33**, 2303765 (2023).
12. Guo, L. et al. Hyperbranched polyborate: a non-conjugated fluorescent polymer with unanticipated high quantum yield and multicolor emission. *Angew. Chem. Int. Ed.* **61**, e202204383 (2022).
13. Zhang, Z. et al. Oxygen and sulfur-based pure n-electron dendrimeric systems: generation-dependent clusteroluminescence towards multicolor cell imaging and molecular ruler. *Sci. China Chem.* **64**, 1990–1998 (2021).
14. Zhang, H. et al. Clusterization-triggered emission: uncommon luminescence from common materials. *Mater. Today* **32**, 275–292 (2020).
15. Wang, Z. et al. Enzyme-inspired nanoreactor containing light-controlled “trojan horse” for redox-hypersensitive drug delivery. *Adv. Funct. Mater.* **33**, 2214899 (2023).
16. Ji, X. et al. Anionic polymerization of nonaromatic maleimide to achieve full-color nonconventional luminescence. *Nat. Commun.* **13**, 3717 (2022).
17. Chen, F. et al. Novel boron- and sulfur-doped polycyclic aromatic hydrocarbon as multiple resonance emitter for ultrapure blue thermally activated delayed fluorescence polymers. *Sci. China Chem.* **64**, 547–551 (2021).
18. Liao, P. et al. Clusterization-triggered emission (CTE): one for all, all for one. *Mater. Chem. Front.* **5**, 6693–6717 (2021).
19. Liu, H. et al. Conformation-directed micelle-to-vesicle transition of cholesterol-decorated polypeptide triggered by oxidation. *J. Am. Chem. Soc.* **140**, 6604–6610 (2018).
20. Chen, S., Cheng, S. X. & Zhuo, R. X. Self-assembly strategy for the preparation of polymer-based nanoparticles for drug and gene delivery. *Macromol. Biosci.* **11**, 576–589 (2011).
21. Liu, H. et al. Protein-inspired polymers with metal-site-regulated ordered conformations. *Angew. Chem. Int. Ed.* **135**, e202213 (2023).
22. Zheng, Y. et al. Multiblock copolymers toward segmentation-driven morphological transition. *Macromolecules* **53**, 5992–6001 (2020).
23. Wang, J. et al. Peptide self-assembly: thermodynamics and kinetics. *Chem. Soc. Rev.* **45**, 5589–5604 (2016).
24. Zhao, Z. et al. Sulphur-containing nonaromatic polymers: clustering-triggered emission and luminescence regulation by oxidation. *Polym. Chem.* **10**, 3639–3646 (2019).
25. Liu, B. et al. Polymerization-induced emission. *Mater. Horiz.* **7**, 987–998 (2020).
26. Schnedermann, C. et al. A molecular movie of ultrafast singlet fission. *Nat. Commun.* **10**, 4207 (2019).
27. Liu, Y. et al. All-organic thermally activated delayed fluorescence materials for organic light-emitting diodes. *Nat. Rev. Mater.* **3**, 18020 (2018).
28. Jing, Y. N. et al. Barbier hyperbranching polymerization-induced emission toward facile fabrication of white light-emitting diode and light-harvesting film. *J. Am. Chem. Soc.* **141**, 16839–16848 (2019).
29. Zhou, Y. et al. Intrinsically fluorescent polyureas toward conformation-assisted metamorphosis, discoloration and intracellular drug delivery. *Nat. Commun.* **13**, 4551 (2022).
30. Chen, Y. et al. An easily accessible ionic aggregation-induced emission luminogen with hydrogen-bonding-switchable emission and wash-free imaging ability. *Angew. Chem. Int. Ed.* **57**, 5011–5015 (2018).
31. Wu, S. et al. Urea group-directed organocatalytic asymmetric versatile dihalogenation of alkenes and alkynes. *Nat. Catal.* **4**, 692–702 (2021).
32. Rongworth, R. Fluoroketone hydrates: helix-breaking solvents for polypeptides and proteins. *Nature* **203**, 295–296 (1964).
33. Li, H. et al. Determination of the pKa values of active-center cysteines,cysteines-32 and -35, in Escherichia coli thioredoxin by Raman spectroscopy. *Biochemistry* **32**, 5800–5808 (1993).
34. Zhou, R. et al. Hydrophobic collapse in multidomain protein folding. *Science* **305**, 1605–1609 (2004).
35. Matis, I. et al. An integrated bacterial system for the discovery of chemical rescuers of disease-associated protein misfolding. *Nat. Biomed. Eng.* **1**, 838–852 (2017).
36. Achord, J. M. & Hussey, C. L. Determination of dissolved oxygen in nonaqueous electrochemical solvents. *Anal. Chem.* **52**, 601–602 (1980).
37. Boyd, C. E. et al. *Water Quality: An Introduction*. *Springer Nature* (2019).
38. Shaner, N. C. et al. Improved monomeric red, orange and yellow fluorescent proteins derived from discosoma sp. red fluorescent protein. *Nat. Biotechnol.* **22**, 1567–1572 (2004).
39. Stocker, S. et al. A role for 2-Cys peroxiredoxins in facilitating cytosolic protein thiol oxidation. *Nat. Chem. Biol.* **14**, 148–155 (2018).
40. Carelli, S. et al. Cysteine and glutathione secretion in response to protein disulfide bond formation in the ER. *Science* **277**, 1681–1684 (1997).
41. Wei, H., Zhuo, R. X. & Zhang, X. Z. Design and development of polymeric micelles with cleavable links for intracellular drug delivery. *Prog. Polym. Sci.* **38**, 503–535 (2013).
42. Zhang, J. et al. A mitochondria-targeted turn-on fluorescent probe for the detection of glutathione in living cells. *Biosens. Bioelectron.* **85**, 164–170 (2016).
43. Dong, B. et al. Simultaneous near-infrared and two-photon in vivo imaging of H_2O_2 using a ratiometric fluorescent probe based on the unique oxidative rearrangement of oxonium. *Adv. Mater.* **28**, 8755–8759 (2016).
44. Belousov, V. V. et al. Genetically encoded fluorescent indicator for intracellular hydrogen peroxide. *Nat. Methods* **3**, 281–286 (2006).
45. Zhang, T. et al. CaMKII is a RIP3 substrate mediating ischemia- and oxidative stress-induced myocardial necroptosis. *Nat. Med.* **22**, 175–182 (2016).

46. Ferreira, C. A. et al. Scavenging of reactive oxygen and nitrogen species with nanomaterials. *Nano. Res.* **11**, 4955–4984 (2018).
47. Kaur, R. et al. Synthesis, characterization and evaluation of antioxidant properties of catechin hydrate nanoparticles. *J. Drug Deliv. Sci. Technol.* **39**, 398–407 (2017).
48. Xie, C. et al. Amelioration of Alzheimer's disease pathology by mitophagy inducers identified via machine learning and a cross-species workflow. *Nat. Biomed. Eng.* **6**, 76–93 (2022).
49. Zhang, X. et al. An injectable mitochondria-targeted nanodrug loaded-hydrogel for restoring mitochondrial function and hierarchically attenuating oxidative stress to reduce myocardial ischemia-reperfusion injury. *Biomaterials* **287**, 121656 (2022).
50. Li, X. et al. Thermosensitive *N*-isopropylacrylamide-*N*-propylacrylamide-vinyl pyrrolidone terpolymers: synthesis, characterization and preliminary application as embolic agents. *Biomaterials* **26**, 7002–7011 (2005).
51. Yao, Y. et al. Reactive oxygen species (ROS)-responsive biomaterials –––mediate tissue microenvironments and tissue regeneration. *J. Mater. Chem. B.* **7**, 5019–5037 (2019).
52. Lepetsos, P. & Papavassiliou, A. G. ROS/oxidative stress signaling in osteoarthritis. *BBA Mol. Basis Dis.* **1862**, 576–591 (2016).
53. Setti, T. et al. The protective role of glutathione in osteoarthritis. *J. Clin. Orthop. Trauma.* **15**, 145–151 (2021).
54. Giustarini, D. et al. How to increase cellular glutathione. *Antioxidants* **12**, 1094 (2023).
55. Song, W. F. et al. Self-assembled copper-based nanoparticles for glutathione activated and enzymatic cascade-enhanced ferroptosis and immunotherapy in cancer treatment. *Small* **19**, 2301148 (2023).

Acknowledgements

This work was supported by the National Natural Science Foundation of China (52022062, 52473313, 52273140, 51873118), the Application and Basic Research of Sichuan Department of Science and Technology, the Project of State Key Laboratory of Polymer Materials Engineering, and the Fundamental Research Funds for the Central Universities.

Author contributions

C.P., Y.Z., and M.D. conceived and designed the research. C.P. and Y.Z. synthesized and characterized the materials. C.P., Y.Z., and Y.Z. performed the fluorescent studies and data analysis. C.P. and K.Z. performed the in vitro and in vivo studies. Y.L., Y.W., C.P., and M.D. performed simulations and calculations. C.P. and M.D. wrote the manuscript with feedback from all the authors. M.D. devised the study and supervised the project with W.F., H.T., and Q.F. All authors discussed the results and commented on the manuscript.

Competing interests

The authors declare no competing interests.

Additional information

Supplementary information The online version contains supplementary material available at https://doi.org/10.1038/s41467-024-54473-x.

Correspondence and requests for materials should be addressed to Weili Fu or Mingming Ding.

Peer review information *Nature Communications* thanks the anonymous reviewers for their contribution to the peer review of this work. A peer review file is available.